Letter    Editors' Suggestion

# Employing quasidegenerate optical modes for chiral sensing

S. F. Almousa [1,2] T. Weiss,[3,4] and E. A. Muljarov[1]

[1]*School of Physics and Astronomy, Cardiff University, Cardiff CF24 3AA, United Kingdom*
[2]*Department of Physics and Astronomy, King Saud University, Riyadh 11451, Saudi Arabia*
[3]*4th Physics Institute and SCoPE, University of Stuttgart, Pfaffenwaldring 57, 70569 Stuttgart, Germany*
[4]*Institute of Physics, University of Graz, and NAWI Graz, Universitätsplatz 5, 8010 Graz, Austria*

Chiral molecules cannot be superposed with their own mirror image. This yields two enantiomers of opposite handedness that are made out of the same building blocks, but interact differently with their environment. Hence, chiral sensing is of utmost importance for biology, chemistry, and life sciences. However, the impact of the handedness and chirality is very weak in most sensing schemes. Nevertheless, it has been demonstrated recently that chirality may result in strong coupling between resonant states with high quality factors. This is achieved by spectrally overlapping two quasibound states in the continuum in a periodic array of nanostructures. We demonstrate that this requires neither quasibound states in the continuum nor periodic arrays, which is exemplified for three achiral systems: a sphere with equal permittivity and permeability, a single core-shell structure, and a dielectric metasurface. For such achiral systems, we have shown previously that isolated resonant states exhibit a quadratic energy shift in the Pasteur parameter. However, for quasidegenerate states, we observe, using the rigorous resonant-state expansion and full-wave simulations, a linear energy shift and linear splitting in the presence of a chiral medium or molecule. Thus, the splitting is more sensitive to low concentrations of chiral molecules, which paves the way for novel chiral sensing schemes.

The pivotal role of chirality in biology, chemistry, and life sciences generates a wide interest in improving chiral sensors. For instance, the interaction of chiral molecules with the human body may depend on the molecular handedness, which is of utmost importance in drug development [1]. Common optical sensors are based on chiral properties of light [2]. The most prominent approach is to determine the so-called circular dichroism as the absorption difference between left- and right-handed circularly polarized incident plane waves [3,4]. However, chiral light-matter interaction is rather weak. Hence, designing chirality sensors essentially requires enhancing the optical response of chiral substances.

Nanophotonic systems are known to resonantly enhance light-matter interaction [5–9]. Quite naturally, researchers started investigating the application of chiral and achiral nanostructures for chiral sensing [10–12]. In 2010, Tang and Cohen introduced local optical chirality as a measure for the absorption difference of chiral molecules with opposite handedness in nontrivial local environments [13]. Since then, this quantity has been used to optimize chiral nanophotonic sensors [14]. An interesting concept is suggested by Feis *et al.*, who designed a cavity with only one handedness of local optical chirality [15]. More recently, we have developed a rigorous theory of chiral sensing using the resonant states

(RSs) of nanophotonic systems [16]. A major finding of this work is that resonance shifts, which dominate in conventional nanophotonic sensors [9], do not contribute to chiral sensors in first order when considering achiral nanostructures. However, we have not considered in our analysis a situation that two or more RSs can be degenerate. Later on, Chen *et al.* demonstrated [17] that nearly degenerate modes can be strongly coupled even by a weak chirality if the initial energy splitting is low and the quality factor (Q-factor) of the modes is high. Such modes with high Q-factors can be obtained when slightly perturbing a system that exhibits bound states in the continuum. Under ideal conditions, these states do not couple to the far field due to symmetry constraints or the radiative loss is suppressed destructively by coupling several RSs [18,19]. The perturbation allows the bound states to couple to the far field, so that they become effectively quasibound states with a high Q-factor. However, bound states in the continuum can be achieved mostly in periodic arrays of nanostructures, except for some exotic situations [20].

We demonstrate now that neither periodic arrays nor extremely high Q-factors are necessary to achieve the strong coupling of nearly degenerate modes. Moreover, using the resonant-state expansion (RSE) based on the correct RS normalization, we rigorously derive a linear energy splitting of quasidegenerate RSs. Although our proposed designs do not allow us to discriminate between the handedness of chiral molecules, this does not diminish the practical significance of our work, as one may need to measure the concentration of a known substance, with a known handedness. The proposed designs result in a concentration-dependent linear

energy shift, which can be used in chiral sensing. More specifically, in a homogeneous chiral medium, the concentration of chiral molecules with same handedness is proportional to the so-called Pasteur parameter $\varkappa$, which is usually extremely small with the values of $\varkappa$ reaching $10^{-4}$–$10^{-3}$ [2]. If the chirality-induced energy shift is a second-order effect in $\varkappa$, the energy shifts scale as $10^{-8}$–$10^{-6}$. However, if two or more optical modes are spectrally very close, i.e., are quasidegenerate, the energy splitting becomes linear and therefore is much more sensitive to chiral perturbations.

In this Letter, we employ quasidegenerate modes of three optical systems to demonstrate a significant chiral energy splitting of the modes and its linear dependence on the Pasteur parameter $\varkappa$. We start with a proof of principle for strictly degenerate optical modes of orthogonal polarizations in a homogeneous sphere with identical material permittivity and permeability. Then, we provide practically more relevant examples of optical systems containing quasidegenerate modes, such as a core-shell dielectric sphere [21,22] and a planar metasurface, which has been initially introduced by Staude *et al.* [23]. Using the RSE [24] and its recent generalization to magnetic, bianisotropic, and chiral systems [25], we obtain an analytic expression for the optical resonances. Accompanied by numerical simulations, we demonstrate a strong linear chiral splitting of quasidegenerate modes of different polarizations in the presence of a chiral medium or a chiral molecule. The results presented below show that the chiral sensitivity of optical systems can be enhanced in this way by orders of magnitude.

The optical modes (also known as RSs or quasinormal modes) of an electromagnetic system are the eigensolutions of Maxwell's equations (in Gaussian units),

$$\nabla \times \mathbf{E} = ik\mathbf{B}, \quad \nabla \times \mathbf{H} = -ik\mathbf{D}, \quad (1)$$

satisfying outgoing boundary conditions. Here, $\mathbf{E}$ and $\mathbf{H}$ are, respectively, the electric and magnetic fields of the RS, and $k$ is its complex wave number in vacuum. Assuming no spatial dispersion of the medium, the electric displacement $\mathbf{D}$ and magnetic induction $\mathbf{B}$ are given by

$$\mathbf{D} = (\hat{\boldsymbol{\varepsilon}} + \Delta\hat{\boldsymbol{\varepsilon}})\mathbf{E} - i(\hat{\boldsymbol{\varkappa}} + \Delta\hat{\boldsymbol{\varkappa}})\mathbf{H},$$
$$\mathbf{B} = (\hat{\boldsymbol{\mu}} + \Delta\hat{\boldsymbol{\mu}})\mathbf{H} + i(\hat{\boldsymbol{\varkappa}} + \Delta\hat{\boldsymbol{\varkappa}})^{\mathrm{T}}\mathbf{E}, \quad (2)$$

where frequency-dispersive and spatially dependent $\hat{\boldsymbol{\varepsilon}}$, $\hat{\boldsymbol{\mu}}$, and $\hat{\boldsymbol{\varkappa}}$ are, respectively, the permittivity, permeability, and chirality tensors, the latter being a generalization of the Pasteur parameter for anisotropic media (T denotes the matrix transpose). Furthermore, $\Delta\hat{\boldsymbol{\varepsilon}}$, $\Delta\hat{\boldsymbol{\mu}}$, and $\Delta\hat{\boldsymbol{\varkappa}}$ are arbitrary perturbations of these tensors. Introducing a complete set of properly normalized [24,25] unperturbed RSs with the wave number $k_n$ and resonant fields $\mathbf{E}_n$ and $\mathbf{H}_n$, satisfying Eqs. (1) and (2) for $\Delta\hat{\boldsymbol{\varepsilon}} = \Delta\hat{\boldsymbol{\mu}} = \Delta\hat{\boldsymbol{\varkappa}} = 0$, where $n$ is an index labeling them, the perturbed RSs can be expanded as

$$\mathbf{E} = \sum_n c_n\mathbf{E}_n, \quad \mathbf{H} = \sum_n c_n\mathbf{H}_n, \quad (3)$$

which effectively maps Eqs. (1) and (2) onto the linear matrix eigenvalue problem [25]

$$(k - k_n)c_n = -k\sum_{n'} V_{nn'}c_{n'}, \quad (4)$$

where

$$V_{nn'} = \int [\mathbf{E}_n \cdot \Delta\hat{\boldsymbol{\varepsilon}}\mathbf{E}_{n'} - \mathbf{H}_n \cdot \Delta\hat{\boldsymbol{\mu}}\mathbf{H}_{n'}]d\mathbf{r}$$
$$-i\int [\mathbf{E}_n \cdot \Delta\hat{\boldsymbol{\varkappa}}\mathbf{H}_{n'} + \mathbf{E}_{n'} \cdot \Delta\hat{\boldsymbol{\varkappa}}\mathbf{H}_n]d\mathbf{r}. \quad (5)$$

For the sake of clarity, the expressions Eqs. (4) and (5) are given for nondispersive and reciprocal systems, although perturbations included in Eq. (5) may be nonreciprocal, and a generalization of Eq. (4) to dispersive systems has been developed [25,26].

To verify Eq. (4), we have taken a large number of basis RSs for the analytically solvable problem of a homogeneous achiral sphere with isotropic permittivity $\varepsilon$ and permeability $\mu$, that is surrounded by vacuum. Then, we applied arbitrarily strong (but finite) homogeneous perturbations of the sphere, $\Delta\varepsilon$, $\Delta\mu$, and $\Delta\varkappa$, also allowing exact analytic solutions. Results demonstrate [27,28] a quick convergence of the RSE to the exact solution, with the relative error in the RS wave numbers $k$ decreasing as inverse cubic law in the basis size, which is the same as demonstrated for dielectric perturbations of a sphere [24].

Then, we consider chiral perturbations of degenerate RSs in an achiral homogeneous and isotropic sphere having the same values for permittivity and permeability, resulting in identical spectra of transverse electric (TE) and transverse magnetic (TM) optical modes (in addition to the $2l + 1$ degeneracy of each mode due to the spherical symmetry). The surrounding of the sphere is assumed to be vacuum, and we select the permittivity and permeability of the sphere to be $\varepsilon = \mu = 4$. For the angular momentum quantum number of $l = 5$, the spectrum of the degenerate TE and TM modes is shown in Fig. 1(a). Focusing on the fundamental whispering-gallery mode (WGM) for this $l$, we see in the right inset that the electric field of the TE mode is identical to the magnetic field of the TM mode and vice versa. This degeneracy is lifted under permittivity or chirality perturbation ($\Delta\varepsilon$ or $\Delta\varkappa = \varkappa$), or both perturbations applied together, see the left inset in Fig. 1(a). Both the unperturbed and perturbed problems have exact analytical solutions. The exact real part of the wave-number splitting of the formerly degenerate RSs is shown in Fig. 1(b) when applying small chiral perturbations, with the Pasteur parameter $\varkappa$ increasing up to nearly $10^{-3}$. We consider three scenarios: homogeneous internal (over the entire volume of the sphere, black lines) and external chiral perturbation (of the surrounding medium, blue lines), as well as internal chiral perturbation of the RSs which are initially split by a small permittivity perturbation $\Delta\varepsilon = 0.01$ of the sphere (green lines). While the black and blue lines exhibit a linear splitting that is larger for internal perturbations due to higher values of the mode fields inside the sphere, the green curve starts quadratically in $\varkappa$ and approaches a linear dependence when the chiral splitting exceeds the initial permittivity splitting of the degenerate modes. Defining the chiral sensitivity as $dk_n/d\varkappa$, and calculating the ratio of this sensitivity between the degenerate (black curve) and nondegenerate (green curve) initial parameters, we obtained the sensitivity enhancement (right axis) as the red curve in Fig. 2(b). It is large for small $\kappa$ values and reaches unity for $\kappa \approx 5 \times 10^{-4}$.
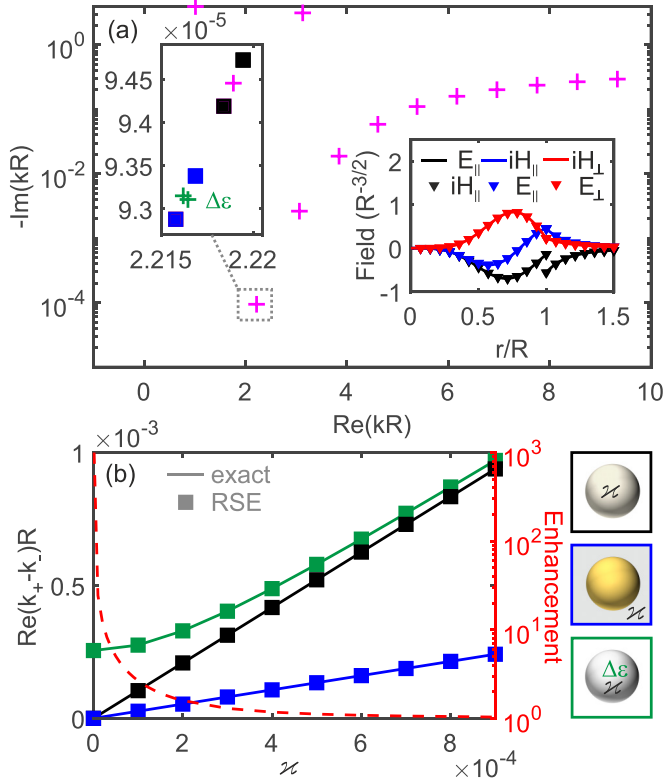
FIG. 1. (a) Wave numbers (magenta crosses) of strictly degenerate TE and TM RSs with angular momentum number $l = 5$ of a basis sphere of radius $R$ and $\varepsilon = \mu = 4$, surrounded by vacuum. Right inset: radial dependence of tangential ($\parallel$) and normal ($\perp$) components of the normalized electric and magnetic fields of the fundamental WGM in TE (lines) and TM (triangles) polarizations, as defined in Eq. (28) of Ref. [29]. Left inset: Unperturbed degenerate (magenta cross) and perturbed split wave numbers of the fundamental WGM due to the dielectric ($\Delta\varepsilon = 0.01$, green crosses), chiral ($\varkappa = 10^{-3}$, black squares), and simultaneous dielectric and chiral ($\Delta\varepsilon = 0.01$, $\varkappa = 10^{-3}$, blue squares) homogeneous perturbations of the basis sphere. (b) Real part of the wave-number splitting, $k_+ - k_-$ (left axis), of the TE-TM degenerate fundamental WGM as a function of the Pasteur parameter $\varkappa$ for chiral perturbations of the sphere (black), vacuum (blue), and sphere with an additional perturbation $\Delta\varepsilon = 0.01$ (green), with the black-to-green chiral sensitivity enhancement factor (red, right axis, see main text for details) and the corresponding sketches of the system given on the right. Solid lines and squares are, respectively, the exact results and the RSE solution given by Eq. (7).

To better understand this behavior, we truncate the exact RSE Eq. (4) to a $2 \times 2$ matrix problem, keeping in the basis only two quasidegenerate RSs [30] having the unperturbed wave numbers $k_1$ and $k_2$. This results in

$$k \begin{pmatrix} 1 + V_{11} & V_{12} \\ V_{21} & 1 + V_{22} \end{pmatrix} \begin{pmatrix} c_1 \\ c_2 \end{pmatrix} = \begin{pmatrix} k_1 & 0 \\ 0 & k_2 \end{pmatrix} \begin{pmatrix} c_1 \\ c_2 \end{pmatrix}. \quad (6)$$

This truncation is justified by second-order perturbation theory corrections [31] to the inverse wave number, $|V_{1n}^2/(k_1 - k_n)/4|$ and $|V_{2n}^2/(k_2 - k_n)/4|$, for all the neglected modes $n$ being small compared to the RS wave-number change $|\Delta k/k^2|$ due to the perturbation. The truncated eigenvalue problem
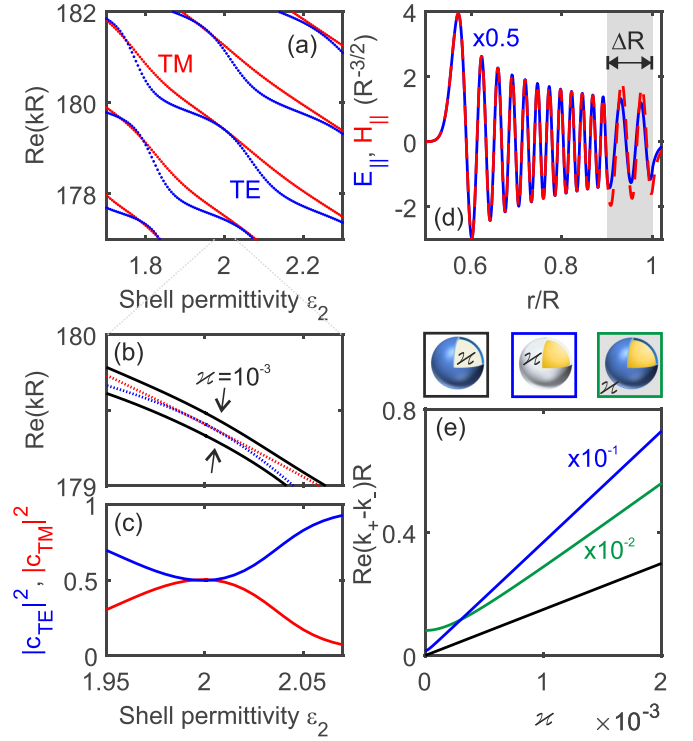


FIG. 2. (a) Real part of the wave numbers of $l = 200$ TE (blue) and TM (red) WGMs of a basis core-shell system, surrounded by vacuum, with $\varepsilon_1 = 4$ in the core, shell thickness $\Delta R = 0.1R$, and system radius $R$, as functions of the shell permittivity $\varepsilon_2$. (b) Real part of the unperturbed (dashed lines) and perturbed (black solid lines) wave numbers, and (c) square moduli of the TE (blue) and TM (red) expansion coefficients in Eq. (6) of the perturbed lower branch as functions of $\varepsilon_2$, for a homogeneous chiral core perturbation of $\varkappa = 10^{-3}$. (d) Real part of the normalized electric field of TE (blue) and the imaginary part of the magnetic field of TM (red) WGMs of the core-shell system at $\varepsilon_2 = 2$. The wave numbers of the TE and TM modes are, respectively, $k_1 R = 179.409265396 - 3.08 \times 10^{-7}i$ and $k_2 R = 179.408443931 - 3.69 \times 10^{-7}i$. (e) Real part of the wave-number splitting, $k_+ - k_-$, of the TE-TM quasidegenerate WGMs in (d), as a function of the Pasteur parameter $\varkappa$ for chiral perturbations of the core (black), shell (blue), and vacuum (green), with the corresponding sketches of the system given on the top. Note that the blue curves in (d) and (e) and the green one in (e) have been rescaled for the sake of clarity. The actual results can be obtained by multiplying the curves with the same-color factors.

Eq. (6) has the explicit solution $k = k_\pm$, where

$$k_\pm = \frac{\tilde{k}_1 + \tilde{k}_2 \pm \sqrt{(\tilde{k}_1 - \tilde{k}_2)^2 + 4k_1 k_2 V_{12} V_{21}}}{2(1 + V_{11} + V_{22} + V_{11}V_{22} - V_{12}V_{21})} \quad (7)$$

with $\tilde{k}_1 = k_1(1 + V_{22})$ and $\tilde{k}_2 = k_2(1 + V_{11})$.

In general, in achiral (i.e., parity symmetric) systems, the chirality $\varkappa$ does not contribute to the diagonal matrix elements in Eq. (5) if the chiral distribution in space does not break the parity symmetry of the system [16]. Furthermore, in spherically symmetric systems, the electric and magnetic fields of the same RS are orthogonal at any point. Therefore, the diagonal elements are present only due to permittivity and/or permeability perturbations. Without those perturbations, $V_{11} = V_{22} = 0$, and the solution Eq. (7)

simplifies to

$$k_\pm = \frac{k_1 + k_2 \pm \sqrt{(k_1 - k_2)^2 + 4k_1 k_2 V_{12} V_{21}}}{2(1 - V_{12} V_{21})}. \qquad (8)$$

Moreover, the mutual orthogonality of electric or magnetic fields for different polarizations makes the off-diagonal elements $V_{12}$ in Eq. (7) dependent on the chirality only and proportional to $\varkappa$. As a result, for small $\varkappa$, the splitting changes quadratically with $\varkappa$, as it is clear from Eqs. (7) and (8). If the two basis modes are strictly degenerate, i.e., $k_1 = k_2$, Eq. (8) simplifies further to

$$k_\pm = \frac{k_1}{1 \mp V_{12}}, \qquad (9)$$

using the general symmetry $V_{nn'} = V_{n'n}$ valid for reciprocal systems. Clearly, for small perturbations, the mode splitting $k_+ - k_- \approx 2k_1 V_{12}$ is *linear* in the Pasteur parameter $\varkappa$. This fact has been implicitly used by Chen *et al.* to demonstrate strong coupling induced by $\varkappa$ [17].

The above analysis clearly explains the behavior of the mode splitting in Fig. 1(b), in which the two-state RSE solution given by Eq. (7) is shown by squares and has errors compared to the exact solution (lines) that scale quadratically with the perturbation strength, in agreement with the mentioned second-order corrections. Note that the RSE in its original form of Eq. (4) works only for internal perturbations. Nevertheless, external perturbations can be treated in the same way to first order, as has been recently shown in Refs. [32,33], provided that the divergent matrix elements are evaluated by applying a proper (in the present case, analytical) regularization [32].

Now we examine a more realistic optical resonator that also allows exact analytical solutions. It consists of a dielectric sphere with permittivity $\varepsilon_1 = 4$ coated by a homogeneous thin layer of thickness $\Delta R = 0.1R$ and variable permittivity $\varepsilon_2$, with $R$ being the outer radius of this nonmagnetic ($\mu = 1$) spherical core-shell system surrounded by vacuum. The shell at least partially compensates the difference between Maxwell's boundary conditions in TE and TM polarizations, which allows the real parts of the RS wave numbers of the opposite polarization to approach each other or even cross, see Fig. 2(a). If additionally the Q-factors of the RSs are high, which is the case for WGMs with large angular momentum (here, $l = 200$ and the Q-factors are about $3 \times 10^8$), these TE and TM modes become quasidegenerate at selective values of the system parameters. Choosing such a TE-TM pair of modes, having the splitting of $|k_1 - k_2|R \approx 8.2 \times 10^{-4}$ at $\varepsilon_2 = 2$, we calculate, using Eq. (8), changes of their wave numbers by homogeneous chiral perturbations of the core, shell, and the surrounding medium (vacuum). The normalized (according to Refs. [25,29]) electric field of the TE mode and the magnetic field of the TM mode, shown in Fig. 2(d), are in fact very similar, at least in the core region, with a proportionality factor of 2 due to $\sqrt{\varepsilon_1/\mu} = 2$ affecting their normalization.

In Fig. 2(b), we display the chiral splitting and anticrossing of the selected pair of modes due to a chirality perturbation of $\varkappa = 10^{-3}$ of the core. As chirality couples the electric and magnetic fields, the perturbed modes are a mixture of
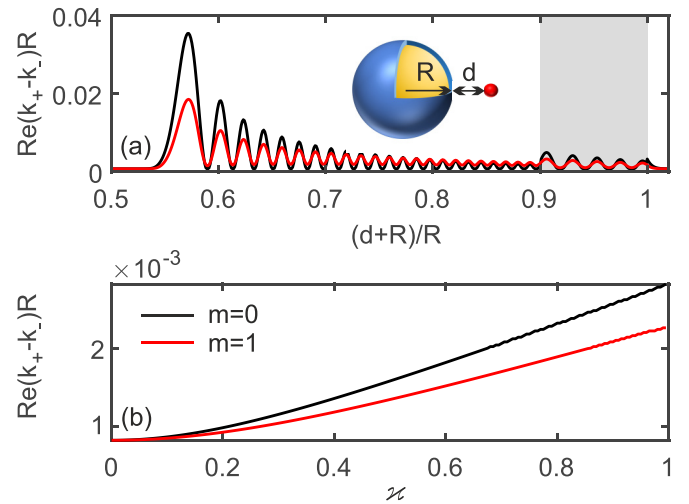


FIG. 3. (a) Real part of the wave-number splitting, $k_+ - k_-$, for the TE-TM quasidegenerate WGMs in Fig. 2(d) with magnetic quantum numbers $m = 0$ (black) and $m = \pm 1$ (red), perturbed by a chiral molecule with effective volume $\mathcal{V}_p/\mathcal{V} = 10^{-7}$ and $\varkappa = 1$ placed near the shell at a distance $d$, as a function of normalized center distance $(d + R)/R$. (b) As in (a), but as a function of $\varkappa$ for $d = -0.005R$.

TE and TM polarizations. This is shown in Fig. 2(c) as the absolute square of the expansion coefficients, both reaching $1/2$ at $\varepsilon_2 = 2$, where the basis mode splitting is minimized. Interestingly, as the wave numbers do not cross, the expansion coefficients do not exhibit the typical strong coupling behavior which would be their crossing and exchange of the mode properties as the detuning parameter (here, the shell permittivity) changes. We see instead that their square moduli stay either below or above $1/2$ everywhere in spite of the strong coupling. This is in stark contrast to the $\varkappa$-mediated strong coupling reported previously [17].

The mode splitting at $\varepsilon_2 = 2$ is shown in Fig. 2(e) as a function of $\varkappa$ for the core, shell, and surrounding-medium perturbations, demonstrating that the chiral splitting falls approximately one order of magnitude in each case in this sequence. The smaller values of the chiral mode splitting for the shell and the surrounding-medium perturbations can be understood, respectively, in terms of a smaller shell volume and smaller values of the fields in the exterior, as it is clear from Fig. 2(d). Consequently, the strong and the intermediate splittings due to, respectively, the chiral core and shell are both linear in the displayed range of $\varkappa$, but the weak splitting for the chiral surrounding appears quadratic at small $\varkappa$ where the chiral perturbation of the modal wave numbers is smaller than or comparable to the initial mode splitting, in agrement with our analysis of Eq. (6).

We also looked at the same core-shell system at $\varepsilon_2 = 2$, perturbed by a chiral particle, with distance $d$ from the sphere surface, see a sketch in Fig. 3(a). The perturbed system has a cylindrical symmetry, so the RSs with different magnetic quantum numbers $m$ are perturbed differently. However, owing to additional selection rules for TE and TM modes with the same $l$, only $m = 0$ and $m = \pm 1$ states are perturbed by the chiral molecule, with the matrix elements given, respectively, by $V_{12} = -2i\varkappa\mathcal{V}_p\beta\mathbf{H}_\perp^{TE} \cdot \mathbf{E}_\perp^{TM}$ and
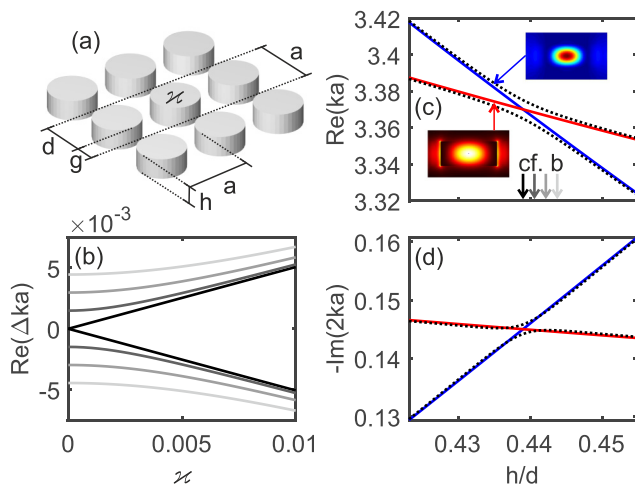
FIG. 4. (a) Schematic of a dielectric metasurface of high-index disks ($n_r = 3.5$) with diameter $d$, period $a$, height $h$, and interparticle distance $g$. (b) Splitting of the wave number as a function of Pasteur parameter $\varkappa$. The splitting typically starts quadratically (gray lines), except for the case of quasidegeneracy (black lines), for which we have fine-tuned all parameters except for the refractive index of the disk. (c) Real and (d) imaginary parts of the wave numbers of the electric (red lines) and magnetic (blue lines) dipolar modes as a function of aspect ratio $h/d$ for $d = 505.1$ nm, $g = 222.8$ nm, and a surrounding medium with $n_r = 1.498$. The quasidegeneracy occurs for $h = 221.7$ nm. Insets in (c) show the resonant magnetic (top) and electric (bottom) fields of the magnetic and electric dipole mode, respectively, at $h = 219.7$ nm, while arrows mark the aspect ratios for the curves in (b).

$V_{12} = -i\varkappa \mathcal{V}_p \beta (\mathbf{E}_{\parallel}^{\mathrm{TE}} \cdot \mathbf{H}_{\parallel}^{\mathrm{TM}} + \mathbf{H}_{\parallel}^{\mathrm{TE}} \cdot \mathbf{E}_{\parallel}^{\mathrm{TM}})$, where $\mathcal{V}_p$ is an effective molecule volume and $\beta = (2l + 1)/(4\pi)$ is a geometrical factor. The TE-TM mode splitting is shown in Fig. 3(a) for $\varkappa = 1$ and $\mathcal{V}_p/\mathcal{V} = 10^{-7}$ ($\mathcal{V} = 4\pi R^3/3$ is the system volume) as a function of normalized center distance $(d + R)/R$. The splitting oscillates with $d$, as it is roughly proportional to the square of the mode field, see Fig. 2(d). The dependence of the splitting on the Pasteur parameter $\varkappa$ for $d = -0.005R$ (inside the core shell) is displayed in Fig. 3(b), demonstrating qualitatively the same behavior as in the previous examples, but quantitatively different for different $m$.

As our last example, we consider a metasurface introduced by Staude *et al.* [23]. The system consists of disks with diameter $d$ and height $h$, which are repeated periodically with period $a = d + g$ in both directions, where $g$ denotes the gap between two neighboring disks. The nonmagnetic disks have a refractive index of $n_r = 3.5$, and the surrounding is glass with an index of $n_r \approx 1.5$. The geometry is depicted in Fig. 4(a). At normal incidence, the system exhibits electric and magnetic dipole resonances in close spectral vicinity for $h \approx 220$ nm, $g \approx 200$ nm, and $d \approx 500$ nm around a wavelength of 1400 nm [23]. For these parameters, the real parts of the resonant wave numbers match, while the imaginary parts are slightly different. We have fine-tuned the parameters to achieve a quasidegeneracy even in the imaginary part, which appears for $h = 221.7$ nm, $g = 222.8$ nm, and $d = 505.1$ nm for a surrounding medium with $n_r = 1.498$. The quasidegeneracy is seen in Fig. 4, where we kept all the parameters the same except for the aspect ratio, and plotted the real and imaginary parts of $ka$ in Figs. 4(c) and 4(d), respectively. The calculations have been carried out via our in-house implementation of the Fourier-modal method [7,34,35]. Next, we artificially added chirality in the form of a Pasteur parameter $\varkappa$ to the disks. At the quasidegeneracy, the energy splitting turns out to be linear in $\varkappa$, see black lines in Fig. 4(b), as expected from the previous analysis. In contrast, if we increase the height in steps of 0.8 nm (gray lines), an intial splitting arises and the splitting starts quadratically. Note that the Q-factor of the quasidegenerate modes in this last example is of the order of 23. Therefore, this example demonstrates strong coupling in spite of the fact that the mode Q-factors are low. Nevertheless, high Q-factors are preferred for a better spectral resolution of the mode splitting.

In conclusion, we have demonstrated linear energy splitting of quasidegenerate modes with respect to the Pasteur parameter $\varkappa$. In the systems treated, the linear splitting is much more sensitive to $\varkappa$ than the usual quadratic onset in the absence of quasidegeneracy. Of course, our proposed systems comprise artificial materials such as solid chiral shells or disks with high refractive index with geometrical parameters that are potentially challenging to realize experimentally. Nevertheless, our numerical and analytical calculations are insightful for improving chiral sensors, and they lift constraints for achieving $\varkappa$-mediated strong coupling compared to the previous work [17].

[1] L. Nguyen and H. He, Int. J. Biomed. Sci. **2**, 85 (2006).

[2] M. Schäferling, *Chiral Nanophotonics* (Springer, Cham, Switzerland, 2017), Vol. 205.

[3] A. J. Miles, R. W. Janes, and B. A. Wallace, Chem. Soc. Rev. **50**, 8400 (2021).

[4] N. Berova, K. Nakanishi, and R. W. Woody, *Circular Dichroism: Principles and Applications* (Wiley, New York, 2000).

[5] S. Arnold, M. Khoshsima, I. Teraoka, S. Holler, and F. Vollmer, Opt. Lett. **28**, 272 (2003).

[6] A. Unger and M. Kreiter, J. Phys. Chem. C **113**, 12243 (2009).

[7] T. Weiss, M. Mesch, M. Schäferling, H. Giessen, W. Langbein, and E. A. Muljarov, Phys. Rev. Lett. **116**, 237401 (2016).

[8] M. Mesch, T. Weiss, M. Schäferling, M. Hentschel, R. S. Hegde, and H. Giessen, ACS Sens. **3**, 960 (2018).

[9] S. Both and T. Weiss, Semicond. Sci. Technol. **37**, 013002 (2022).

[10] E. Hendry, T. Carpy, J. Johnston, M. Popland, R. V. Mikhaylovskiy, A. J. Lapthorn, S. M. Kelly, L. D. Barron, N. Gadegaard, and M. Kadodwala, Nat. Nanotechnol. **5**, 783 (2010).

[11] A. O. Govorov, Z. Fan, P. Hernández, J. M. Slocik, and R. R. Naik, Nano Lett. **10**, 1374 (2010).

[12] A. O. Govorov and Z. Fan, Chem. Phys. Chem. **13**, 2551 (2012).

[13] Y. Tang and A. E. Cohen, Phys. Rev. Lett. **104**, 163901 (2010).

[14] M. Schäferling, D. Dregely, M. Hentschel, and H. Giessen, Phys. Rev. X **2**, 031010 (2012).

[15] J. Feis, D. Beutel, J. Köpfler, X. Garcia-Santiago, C. Rockstuhl, M. Wegener, and I. Fernandez-Corbaton, Phys. Rev. Lett. **124**, 033201 (2020).

[16] S. Both, M. Schäferling, F. Sterl, E. A. Muljarov, H. Giessen, and T. Weiss, ACS Nano **16**, 2822 (2022).

[17] Y. Chen, W. Chen, X. Kong, D. Wu, J. Chu, and C.-W. Qiu, Phys. Rev. Lett. **128**, 146102 (2022).

[18] K. Koshelev, S. Lepeshov, M. Liu, A. Bogdanov, and Y. Kivshar, Phys. Rev. Lett. **121**, 193903 (2018).

[19] S. Neale and E. A. Muljarov, Phys. Rev. B **103**, 155112 (2021).

[20] F. Monticone and A. Alù, Phys. Rev. Lett. **112**, 213903 (2014).

[21] M. G. Silveirinha, Phys. Rev. A **89**, 023813 (2014).

[22] B. Vennes and T. C. Preston, Phys. Rev. A **104**, 033512 (2021).

[23] I. Staude, A. E. Miroshnichenko, M. Decker, N. T. Fofang, S. Liu, E. Gonzales, J. J. Dominguez, T. S. Luk, D. N. Neshev, I. Brener, and Y. S. Kivshar, ACS Nano **7**, 7824 (2013).

[24] E. A. Muljarov, W. Langbein, and R. Zimmermann, Europhys. Lett. **92**, 50010 (2010).

[25] E. A. Muljarov and T. Weiss, Opt. Lett. **43**, 1978 (2018).

[26] E. A. Muljarov and W. Langbein, Phys. Rev. B **93**, 075417 (2016).

[27] E. A. Muljarov and T. Weiss, Photon, Birmingham (2018).

[28] E. A. Muljarov and T. Weiss, 9th International Conference on Metamaterials, Photonic Crystals and Plasmonics, Marseille (2018).

[29] E. A. Muljarov, Phys. Rev. A **101**, 053854 (2020).

[30] T. Weiss, M. Schäferling, H. Giessen, N. A. Gippius, S. G. Tikhodeev, W. Langbein, and E. A. Muljarov, Phys. Rev. B **96**, 045129 (2017).

[31] M. B. Doost, W. Langbein, and E. A. Muljarov, Phys. Rev. A **90**, 013834 (2014).

[32] S. F. Almousa and E. A. Muljarov, Phys. Rev. B **107**, L081401 (2023).

[33] Z. Sztranyovszky, W. Langbein, and E. A. Muljarov, Phys. Rev. Res. **5**, 013209 (2023).

[34] T. Weiss, G. Granet, N. A. Gippius, S. G. Tikhodeev, and H. Giessen, Opt. Express **17**, 8051 (2009).

[35] T. Weiss, N. A. Gippius, S. G. Tikhodeev, G. Granet, and H. Giessen, J. Opt. Soc. Am. A **28**, 238 (2011).